A2A–cAMP–K^+ Pathway Modeling in Dopamine-Depleted Striatal Medium Spiny Neurons

Arabella Troeger[1]

Received December 27, 2025
Accepted August 17, 2026
Electronic access September 30, 2026

Parkinson's disease (PD) is a neurodegenerative disease resulting in motor impairment due to the decline of dopaminergic neurons in the substantia nigra. Adenosine A2A receptor antagonists have been identified as alternative adjunct therapeutic options for Parkinson's disease motor fluctuations, but very few computational models have explicitly integrated A2A receptor signaling, cAMP signaling, and modulation of potassium currents during dopamine depletion. Therefore, a NEURON-based computational model of striatal neurons was implemented, where A2A receptor activation modulates cAMP production and degradation, along with the effects of cAMP on potassium channel conductance under Parkinson's disease conditions. To validate the model, its electrophysiological outputs were compared to published experimental recordings of striatal neuronal excitability. Simulation outputs were compared across conditions using descriptive summaries of run-level variability under small injected current jitter. Under dopamine-depleted conditions, A2A activation produced higher modeled cAMP levels and potassium conductance than the control-like conditions, together with a more negative mean membrane response during stimulation. These results replicate the data trends reported in experimental literature and quantify A2Amediated signaling that drives neuronal excitability in the context of PD, providing a mechanistic avenue to examine the contributions of A2A receptor activity to the pathophysiology of the disease and potentially to guide the development of future pharmacological strategies.

Keywords: Parkinson's disease, adenosine A2A receptor, cAMP, potassium conductance, computational modeling, NEURON.

Introduction

Computational neuronal models are powerful tools that reduce the gap between theoretical neuroscience and experimental findings. In controlled environments, researchers can investigate complex neural pathways in response to stimuli that may be more challenging to replicate experimentally. These models are contributory in studying neurodegenerative diseases such as Parkinson's disease. PD is characterized by the progressive loss of dopaminergic neurons in the substantia nigra, which disrupts signaling in the basal ganglia and leads to motor impairment. While standard treatments such as levodopa are effective in improving motor function, long-term use often results in levodopa-induced dyskinesia. This has led to the exploration of alternatives, such as adenosine A2A receptor antagonists, which have been found to reduce motor complications[1,2]. In the striatum, adenosine A2A receptors play a critical role in modulating dopaminergic signaling in cAMP pathways[3–5]. Adenosine A2A receptor signaling in the striatum is closely linked to dopamine D2 receptor function through well-described antagonistic receptor interactions and heteromeric signaling mechanisms[6] ,providing an important mechanistic basis for modeling A2A effects specifically in indirect-pathway medium spiny neurons. In parallel, the downstream cAMP/PKA/DARPP-32 cascade[7] provides a well-established intracellular framework through which dopamine- and adenosine-dependent signaling can influence striatal excitability and synaptic integration[8]. Although A2A antagonists limit motor complications in advanced PD, few computational models have explicitly integrated into the mechanism linking A2A signaling to cAMP and K^+ conductance changes under dopamine depletion.

Previous striatal models have emphasized dopaminergic modulation while overlooking the cascade between A2A, cAMP, and conductance in the PD state. This gap limits inference regarding how receptor level signaling shapes intrinsic excitability and ultimately therapeutic response.

This study implements a NEURON-based single-compartment medium spiny neuron (MSN) model that links A2A activation to cAMP kinetics and K^+ conductance. This model is sufficient because the objective is to quantify intrinsic (somatic) excitability under identical current injection and to isolate the A2A–cAMP–K^+ conductance mechanism, rather than to model dendritic integration or spatially distributed synaptic inputs. The present reduced formulation is also consistent with prior biophysical and computational work showing that dopaminergic modulation

[1] *Independence High School, Virginia, USA*

strongly shapes MSN integrative properties[9], while more recent literature emphasizes that these effects are cell-type-specific and embedded in broader striatal signaling networks. Accordingly, the present model is intended as a mechanism-isolation framework rather than a full reconstruction of all known striatal signaling complexity. This also explores the implementation of the quantifications of effects on membrane potential, modulated K^+ conductance, K^+ current, and cAMP across Control, PD, and PD + istradefylline. This examination is to validate simulated trends against published in vitro, in vivo, and clinical data.

This model adopts a Hodgkin–Huxley–style membrane formulation combined with a receptor-signaling module that multiplicatively scales g_{mod} as a function of cAMP, thereby linking molecular signaling to intrinsic excitability. This study makes use of a single-compartment model, which necessarily simplifies the complex electrophysiology of the striatal medium spiny neuron. Therefore, predictions do not address dendritic integration or network oscillations. The model is implemented in NEURON, evaluated under identical current injection across the four conditions, and compared using descriptive summaries of run-level outputs under matched stimulation, with trends evaluated against eight published studies spanning cellular, systems, and clinical levels.

Methods

The model of a striatal spiny neuron was created and simulated to learn the contributions of adenosine A2A receptor activity to striatal neuronal excitability under Parkinsonian conditions. All computational modeling was performed using Python 3.13 within the NEURON simulation environment (version 8.2.7; Yale University)[10]. Simulations were executed on a personal computer running Windows 11 with AMD Ryzen 5 5600X 6-Core Processor, 16 GB RAM, and a NVIDIA GeForce RTX 3060 GPU.

Model Architecture and Parameterization

The model represents a single-compartment striatal spiny neuron[11,12], including passive membrane properties and active ion channels to replicate electrophysiological behaviors. The core of the model is a potassium current (k_mod_pd), designed to represent potassium currents under Parkinson's depleted-dopamine conditions. In the present study, this mechanism should be interpreted as a phenomenological delayed- rectifier-like K^+ current, rather than as a molecularly specific channel subtype. This designation is based on the Hodgkin–Huxley-style activation formalism used in the model, including a single activation gate and fourth-order activation term (n^4), which are classically associated with delayed-rectifier formulations. We selected this reduced representation to capture the experimentally supported direction of greater potassium conductance and lower intrinsic excitability under dopamine-depleted, A2A-active conditions—without claiming that one isolated Kv subunit has been uniquely identified as the mediator. This mechanism's conductance relies on intracellular cAMP levels and A2A receptor activation. The potassium activation gate n was initialized to 1.0 at the start of each simulation to reduce startup transients but was subsequently updated using Hodgkin–Huxley-style first-order kinetics $dn/dt = (n_\infty - n)/(T_n)$. It is important to note that for debugging purposes, n was temporarily fixed to 1.0 in earlier iterations of the model to isolate the modulation of potassium conductance (g_{mod}). This debugging adjustment has since been removed in the final version of the model. The potassium current was computed as $ik = g_{mod}(n^{nq})(v - e_k)$. To focus the model on the A2A–cAMP–conductance coupling, we used a single potassium activation gate with standard first-order kinetics and an exponent n_q rather than a multi-state channel model. The reversal potential for potassium (ek) was read directly from NEURON's ion handling system. Baseline passive and intrinsic electrophysiological properties were selected to fall within experimentally reported ranges for neostriatal medium spiny neurons[12], while conductance and signaling parameters specific to this model were defined within the NMODL mechanism and simulation scripts. Mechanism parameters were set in the Python script at runtime (overriding NMODL defaults) to ensure consistent condition definitions. A single-compartment architecture was selected because the purpose of this study was to test how an isolated A2A–cAMP-dependent potassium conductance alters somatic membrane responses under the same injected-current protocol across conditions. Under this reduced framework, all conditions experience identical geometry, passive properties, and stimulus timing, so between-condition differences can be attributed specifically to the modeled signaling-conductance coupling rather than to dendritic filtering, spatial channel gradients, or distributed synaptic inputs. This design is therefore appropriate for a mechanism-isolation study of somatic excitability, but it is not intended to reproduce the full spatial physiology of medium spiny neurons.

Biological Mechanisms Implemented

The model includes several biological mechanisms to simulate the interaction between dopamine depletion, A2A receptor signaling, cAMP dynamics, and potassium current modulation. Dopamine depletion, which characterizes the Parkinsonian state, was represented by a binary state variable, DA_level (1 for normal conditions, 0 for dopamine-depleted, Parkinsonian conditions). Dopamine depletion was modeled to be consistent with known A2A-D2 receptor interactions that shape

adenylyl cyclase signaling[5,13,14]. The activation state of the A2A receptor was controlled by a toggle variable, A2A_on (0 for inactive, 1 for active). When A2A_on was active under dopamine-depleted conditions, it led to a significant increase in cAMP production. The binary DA_{level} could be interpreted as a simplified disease-state indicator, not a quantitative dopamine concentration; its purpose is to capture the qualitative transition from dopamine-intact to dopamine-depleted striatal signaling in which A2A-mediated cAMP elevation becomes disinhibited. Intracellular cAMP concentration was modeled as a dynamic state variable (cAMP) that evolves dynamically based on both production and degradation rates. cAMP production included a basal rate (basal_cAMP_prod) and an A2A-driven component, which was scaled by prod_rate when DA_level was low. The full mathematical formulation of these dynamics is provided below. Under dopamine depletion with A2A activation, the production-degradation balance drives cAMP to the upper bound (saturation) in the untreated PD condition. The baseline maximum potassium conductance was defined as gkbar. The modulated potassium conductance (g_mod) was determined by the A2A activation state and cAMP levels. When A2A was active, $gmod = gkbar \cdot (1 + pd\_cAMP\_gain \cdot (cAMP - base\_cAMP))$. Under control conditions (without A2A activation or dopamine depletion effects), gmod =gkbar. This formulation captures the facilitatory effect of A2A activation, mediated by cAMP, on potassium currents[5,15]. In the present model, this cAMP-dependent modulation is represented phenomenologically rather than through an explicit multi-step biochemical cascade.

Mathematical Formulation of Ion Channel and cAMP Dynamics

To mechanistically link A2A receptor activation to potassium conductance, we implemented a Hodgkin–Huxley–style potassium current coupled to a dynamic intracellular cAMP signaling variable within a custom NMODL mechanism (k_mod_pd). Intracellular cAMP was modeled as a dimensionless, normalized state variable representing relative signaling activity rather than absolute concentration. A value of cAMP = 1 corresponds to baseline signaling, and cAMP was constrained to the range $0 \leq \text{cAMP} \leq 3$ to represent the normalized dynamic range of intracellular signaling activity. All cAMP values reported in tables, figures, and results use this normalized (unitless) scale. All reported cAMP values are therefore unitless and should be interpreted as relative signaling levels, not absolute micromolar concentrations.

Intracellular cAMP concentration was modeled as a first-order dynamic state variable governed by production and degradation processes:

$$dcAMP/dt = A2A_{\text{on}}(1 - DA_{\text{level}}) \cdot \text{prod}_{\text{rate}} + \text{basal\_cAMP\_prod} - \text{deg}_{\text{rate}} \cdot cAMP$$

where:

- $A2A_{on} \in \{0,1\}$ represents A2A receptor activation
- $DA_{level} \in \{0,1\}$ represents dopamine state (1 = control, 0 = dopamine-depleted)
- $prod_{rate}$ is the A2A-driven cAMP production rate under dopamine depletion
- basal_cAMP_prod is a constant basal production rate is the first-order degradation rate

The parameters governing cAMP dynamics were selected to produce stable baseline behavior and controlled signal amplification. Specifically, basal_cAMP_prod and deg_rate determine the steady-state baseline level of cAMP, while prod_rate controls the magnitude of A2A-driven elevation under dopamine depletion[16]. With the chosen values (basal_cAMP_prod = 0.1 and deg_rate = 0.1), the baseline steady state is cAMP ≈ 1.

The control and dopamine depleted states approximate the loss of dopaminergic D2-mediated restraint over the A2A/adenylyl cyclase/cAMP pathway in Parkinsonian striatum, rather than modeling dopamine concentration continuously.

During simulations dopamine-depleted modules were set via the Python driver script as:

$$prod_{rate} = 1.0ms^{-1}, basal\_cAMP\_prod = 0.1ms^{-1}, = 0.1ms^{-1}$$

To maintain physiological plausibility, cAMP was constrained at each timestep to:

Under control conditions, this formulation yields a steady-state value of cAMP=1 , while under dopamine depletion with active A2A signaling, cAMP increases toward the imposed upper bound.

The baseline maximum potassium conductance was defined as gkbar. The modulated potassium conductance (g_mod) was determined by the A2A activation state and intracellular cAMP levels. Specifically, if A2A_on = 1, then $g_{\text{mod}} = g_{k,\text{bar}}\left[1 + \text{pd}_{\text{cAMP\_gain}}(\text{cAMP} - \text{base}_{\text{cAMP}})\right]$; if A2A_on = 0, then g_mod = gkbar. This means that increases in cAMP above the baseline level (base_cAMP) produce proportional increases in potassium conductance only when A2A signaling is active. The parameter pd_cAMP_gain determines how strongly changes in cAMP affect conductance. This formulation implements a linear, phenomenological coupling between intracellular signaling and membrane conductance, allowing cAMP elevation under dopamine depletion to increase potassium current magnitude without explicitly modeling intermediate signaling molecules such as PKA or DARPP-32.

The potassium current was computed as:

where:

- E_K=-90mV is the potassium rersal potential
- n Is the activation gating variable
- the exponent 4 represents a fourth-order activation process consistent with classical delayed rectifier potassium channels, in which multiple independent gating subunits must be activated for channel opening

In this study, $n_q = 4$ was used as a standard Hodgkin–Huxley-style phenomenological assumption for delayed-rectifier-like activation rather than as a fitted parameter for a molecularly identified K^+ channel subtype. The exponent was therefore held constant across all conditions so that between-condition differences would reflect the modeled A2A–cAMP-dependent conductance modulation rather than changes in channel-order assumptions. In the present implementation, E_K was fixed at -90 mV for all conditions and was not varied as a function of intracellular or extracellular K^+ concentration; thus, condition-dependent effects arose from changes in g_{mod} rather than from changes in the K^+ reversal potential.

The activation gate n followed first-order Hodgkin–Huxley kinetics:

with voltage-dependent steady-state activation and time constant defined as:

To ensure numerical stability near singularities, the auxiliary function $vtrap(x, y)$ was used. When the ratio x/y is very small (specifically when the absolute value of x divided by y is less than 10^{-6}), the function is approximated using a first-order Taylor expansion as y multiplied by (1 minus x divided by 2y). This avoids numerical instability caused by division by values close to zero. For all other values of x/y, the function is computed using the standard expression x divided by (exp(x/y) minus 1). This formulation prevents undefined or unstable behavior in the gating rate calculations.

At the start of each simulation, the gating variable was initialized as:

to minimize startup transients. The gating variable was subsequently updated dynamically according to the differential equation above. All mechanism parameters were assigned at runtime via the Python simulation script, overriding default values defined in the NMODL file to ensure consistent experimental conditions across simulations.

Simulation Protocols

Simulations were performed under four labeled conditions: Control Baseline, Control + A2A ON, PD + A2A ON, and PD + Istradefylline. In the model implementation, these correspond to the following toggle states: Control Baseline (DA_level = 1, A2A_on = 0), Control + A2A ON (DA_level = 1, A2A_on = 1), PD + A2A ON (DA_level = 0, A2A_on = 1), and PD + Istradefylline (DA_level = 0, A2A_on = 0). Thus, the PD + Istradefylline condition is implemented computationally as A2A OFF under dopamine depletion. Each condition consisted of 20 simulation runs. Twenty runs per condition were used to quantify within-protocol stability under the imposed small Gaussian jitter in injected current amplitude. Because the model is otherwise deterministic and does not include stochastic channel noise or biological heterogeneity, the purpose of repeated runs was not to estimate population variability, but to characterize the sensitivity of the reported outputs to small input perturbations under fixed model assumptions. In this study, a 'run' refers to one execution of the same deterministic model under a fixed condition, with the only across-run variation arising from the small Gaussian jitter applied to the injected current amplitude (mean 0.2 nA, σ = 0.005 nA). Accordingly, across-run variability in reported metrics reflects input perturbation under the specified protocol rather than biological variability or stochastic channel noise. All reported metrics represent runaveraged values unless otherwise specified. The control conditions represent a healthy striatal neuron with normal dopamine level (DA_level = 1); under this model formulation, A2A activation does not increase cAMP in control (i.e., A2A-driven cAMP production is gated by dopamine depletion), so Control Baseline and Control + A2A ON are expected to be similar. The untreated Parkinsonian condition represents a dopamine-depleted state (DA_level = 0) with A2A signaling enabled, producing elevated cAMP and increased potassium conductance. The treated Parkinsonian condition (PD + Istradefylline) represents A2A receptor antagonism and was modeled by setting A2A_on = 0 under dopamine depletion.

This protocol was selected to compare relative intrinsic excitability across conditions under matched input drive while isolating the effect of the A2A–cAMP–K^+ conductance mechanism. Using the same depolarizing step in all conditions allows differences in membrane potential, potassium current, conductance, and cAMP to be attributed to condition-dependent changes in intrinsic properties rather than to differences in stimulus waveform. During-stimulus metrics were computed over 100–250 ms to capture the early sustained response after stimulus onset, while steady-state metrics over 400–600 ms were used to quantify the late plateau after transient onset effects had decayed. These windows were chosen to distinguish early evoked behavior from stable sustained behavior under continuous current injection. In the PD + A2A ON condition, cAMP rose to the model's upper bound ($\approx$3), increasing g_mod and the magnitude of I_K relative to baseline.

VmAvg was computed as the arithmetic mean of all membrane-potential samples recorded between 100 and 250 ms during the stimulus period. Simulations were performed with a fixed timestep of 0.1 ms (corresponding to a sampling

rate of 10 kHz). No spike removal or filtering was applied; therefore, VmAvg reflects the full membrane-potential trajectory during this interval, including any suprathreshold events. VmAvg represents a during-stimulus metric and should not be interpreted as the resting membrane potential.

Data Analysis and Validation

Simulation outputs were analyzed to assess physiological and molecular metrics. Measured metrics included VmAvg, IKAvg, GmodAvg, and cAMPAvg, computed as during-stimulus averages over 100–250 ms unless otherwise specified. A constant current injection (0.2 nA, 100–600 ms; Gaussian jitter $\sigma = 0.005$ nA across trials) was applied in all simulations. Primary reported metrics were computed over a during Representative time course traces under constant current injection (0.2 nA). Light shading: stimulus (100-600 ms); dark shading: analysis window (100-250 ms). indicates the analysis window (100–250 ms) used for VmAvg and IKAvg. Panels A–D show the time stimulus window of 100–250 ms, and late-stimulus steady-state metrics were computed separately over 400–600 ms during the ongoing current injection. Sensitivity analysis of pd_cAMP_gain. To assess robustness of the modeled condition differences to the strength of cAMP-dependent conductance coupling, we performed a local sensitivity analysis on pd_cAMP_gain, the parameter controlling how strongly deviations in cAMP above baseline scale the modulated potassium conductance. Simulations were repeated across pd_cAMP_gain values of 0, 1, 2.5, 5, 7.5, and 10 while all other parameters and stimulus conditions were held constant. For each tested value, the same four conditions and run structure were used, and VmAvg, IKAvg, GmodAvg, and cAMPAvg were recomputed. Because the present study uses repeated executions of a deterministic model rather than biological replicates, we report across-run distributions descriptively rather than treating them as inferential evidence of population-level statistical significance. For each condition, VmAvg, IKAvg, GmodAvg, and cAMPAvg are summarized as mean ± standard deviation across the 20 simulation runs, together with pairwise mean differences between conditions. In this framework, across-run variability reflects sensitivity to the imposed current jitter under the fixed model assumptions and parameterization, not biological heterogeneity. The purpose of these summaries is therefore to quantify effect magnitude and within-protocol stability of the modeled condition differences. Trial-to-trial variability was addition-

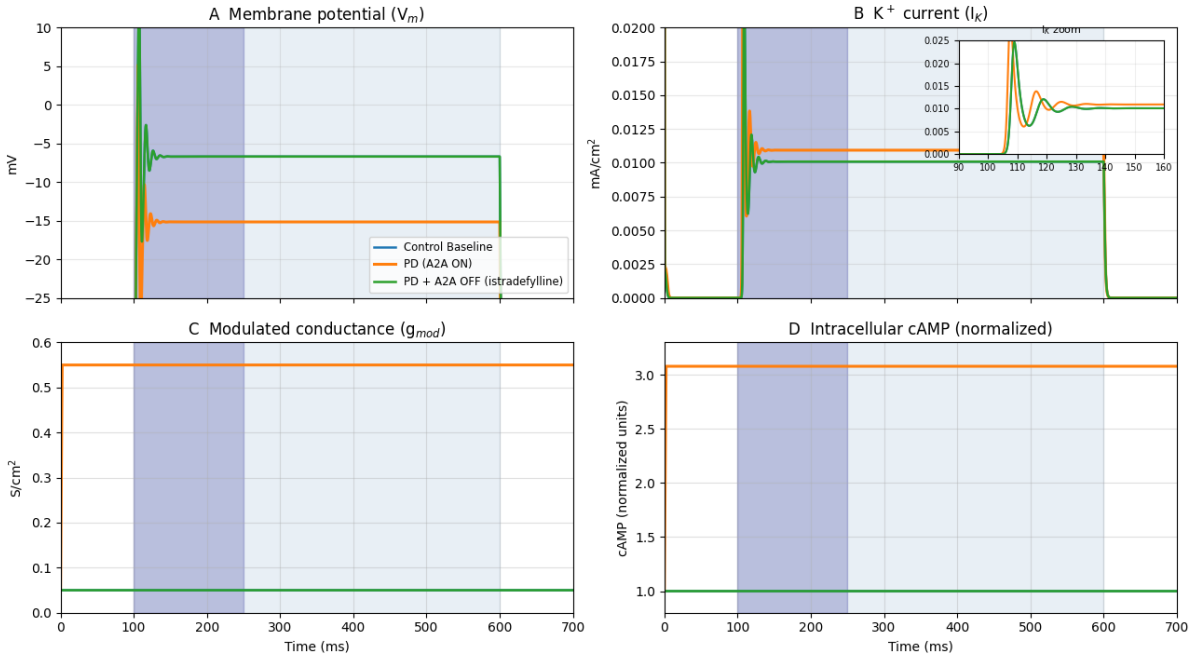

Figure. 1 Representative time-course traces of V_m, I_K, g_mod, and cAMP under constant current injection (0.2 nA). Light shading indicates the stimulus window (100–600 ms), and dark shading indicates the analysis window (100–250 ms) used for Vmavg and Ikavg. Panels A–D show responses for Control Baseline, PD + A2A ON, and PD + ISTRADEFYLLINE (istradefylline). The dashed line in Panel A marks resting membrane potential ($\approx -65mV$). Under PD + A2A ON, elevated cAMP increases potassium conductance and produces a more negative membrane potential, while A2A antagonism restores values toward control.

ally summarized using the coefficient of variation (CV = SD / $|mean| \times 100\%$) across the 20 runs within each condition. In the present study, these CV values should be interpreted as descriptive measures of within-protocol stability under injected-current jitter rather than as estimates of biological population variability. To clarify the strength of evidence supporting different parts of the model, validation sources were classified as direct experimental support, indirect experimental support, or contextual modeling support. Direct support refers to studies that align closely with specific modeled relationships, such as A2A-mediated cAMP signaling and its effect on intrinsic excitability. Indirect support refers to studies that support the broader Parkinsonian or therapeutic context without directly measuring the exact modeled variables or couplings. Contextual support refers to studies that justify the use of a reduced MSN computational framework.

To supplement p-values with a measure of effect magnitude, omnibus between-condition comparisons were summarized using η^2 from one-way ANOVA, and key pairwise contrasts were summarized using Cohen's d. In the present study, these effect sizes are interpreted descriptively as measures of modeled condition separation under the specified simulation protocol, rather than as population-level estimates from biological sampling.

Mechanistic validation was based on experimental data from individual neurons or brain tissue [3–5]. Translational validation, to demonstrate the model's output shows a relation to real Parkinson's patients [2,17]. Contextual validation, to address the model's innovation in computational neuroscience [12,18,19]. Input resistance (Rin) was estimated using small hyperpolarizing current steps (-0.05 nA), computed as the steady-state voltage deflection (ΔV) relative to baseline divided by the applied current (ΔI). In all simulations, a constant current injection with mean amplitude 0.2 nA (Gaussian jitter σ = 0.005 nA) was applied from 100–600 ms (Figure 1) to evoke and sustain a response.

Model Parameters

Table 1 summarizes the key model parameters and their justifications, which were used in the simulations presented throughout this study.

Passive Properties

The foundational properties of single-compartment striatal spiny neurons were modeled after known physiological properties. The specific membrane capacitance (Cm) was set to $1.0 \mu F/cm^2$, a standard value accepted in neuronal modeling, consistent with the work of Hodgkin and Huxley [20]. The axial resistance (Ra) was configured at 100 $\Omega \cdot cm$, a typical value for intracellular resistivity in neuronal processes. A passive (leak) conductance (gpas) of $1 \times 10 - 4 S/cm^2$ and a passive (leak) reversal potential (Epas) of $-65mV$ were set directly within the model script. These values were adjusted to gain an optimal realistic resting membrane potential and input resistance for the model, ensuring fitting threshold behavior. For example, given the soma's dimensions ($20 \mu m$ diameter and $20 \mu m$ length), the whole-cell input resistance (Rin) of the model was approximately $795 M\Omega$, commonly reported ranges, reflecting the simplified single-compartment geometry and passive parameterization of the model. The model's resting membrane potential (Erest) naturally settled at $-65mV$, directly corresponding to the Epas in the absence of other active currents.

All model code and simulation files are publicly available on GitHub.

Link: `https://github.com/RE5275/msn-model-K-channel`

Ethical Considerations

This study involved only computational simulations and did not include human participants, animals, or identifiable private data. Therefore, institutional review board (IRB) or animal care (IACUC) approval and informed consent were not required.

Results

To investigate the effects of adenosine A2A receptor activity on striatal neuron excitability under Parkinsonian conditions, computational simulations were conducted across four labeled conditions: Control Baseline, Control + A2A ON, PD + A2A ON, and PD + Istradefylline. In the model, the PD + Istradefylline condition was implemented by setting A2A_on = 0 under dopamine depletion (DA_level = 0). The physiological and molecular metrics obtained from these simulations are presented below. Figure 1 shows 3 representative traces (Control, PD, PD + istradefylline). Stats include 4 conditions, adding Control + A2A ON (Figure 2). To verify that the model operates within a physiologically realistic regime prior to condition-specific simulations, baseline electrophysiological properties were evaluated. In the absence of current injection, the membrane potential stabilized at approximately 65 mV (Figure 2, Panel A), consistent with the passive leak reversal potential and within experimentally reported ranges for medium spiny neurons. Input resistance was estimated using small hyperpolarizing current steps (-0.05 nA), yielding a value of approximately $795 M\Omega$ (Figure 2, Panel B). While this value lies above the range commonly reported for medium spiny neurons (typically $\sim$100–300$M\Omega$), it reflects the simplified single-compartment geometry and passive parameterization of the model. These results confirm that the

Table 1 Direct support indicates evidence closely aligned with a modeled relationship; indirect support indicates evidence supporting the broader biological or translational interpretation; contextual support indicates evidence supporting the computational framework rather than the specific mechanistic coupling.

Reference	Key finding from cited study	What it supports in the present model	Type of support	Scope of inference
(Rau et al., 2015)[15], (Shen et al., 2013)[5]	Experimental evidence supports A2A-related modulation of cAMP-linked signaling in striatal neurons.	Supports the modeled coupling between A2A activation and increased intracellular cAMP signaling under dopamine-depleted conditions.	Direct experimental support	Supports the direction of the modeled A2A→cAMP effect, but not the exact numerical parameterization used here.
(Calon et al., 2004)[3]	A2A–D2 receptor interactions and adenylyl cyclase-related signaling provide a mechanistic basis for altered cAMP regulation in dopamine-depleted striatum.	Supports the biological rationale for representing dopamine depletion as disinhibition of A2A-mediated cAMP signaling.	Direct experimental support	Supports the pathway logic underlying the disease-state toggle, but not the full reduced mathematical implementation.
(Rau et al., 2015)[15]	Postsynaptic A2A signaling has been linked to regulation of intrinsic excitability and ion-channel-related effects.	Supports the modeled link between elevated A2A/cAMP signaling and altered potassium-conductance-dependent excitability.	Direct experimental support	Supports the mechanism class represented in the model, but does not identify or validate the exact single-channel formulation used here.
(Calon et al., 2004)[3]	Increased A2A receptor expression or signaling has been reported in Parkinsonian tissue.	Supports the disease-context plausibility of stronger A2A-related signaling in PD.	Indirect experimental support	Supports the biological context for enhanced A2A relevance in PD, but does not directly test the modeled A2A→cAMP→K^+ conductance chain.
(LeWitt et al., 2008)[2]	Clinical studies report beneficial effects of istradefylline in Parkinson's disease.	Supports the translational plausibility of the PD + istradefylline condition represented as A2A antagonism in the model.	Indirect experimental support	Supports the treatment interpretation at a clinical level, but does not directly validate the single-cell signaling and conductance mechanism.
(Singh et al., 2016)[17]	In vivo or human electrophysiological studies report altered striatal activity in Parkinson's disease.	Supports the broader physiological relevance of altered neuronal excitability in the Parkinsonian state.	Indirect experimental support	Supports consistency with disease-related changes in neuronal activity, but does not directly validate the specific modeled intracellular mechanism.
(Gertler et al., 2008)[11], (Wilson and Kawaguchi, 1996)[12]	Prior computational MSN studies provide biophysical and architectural context for reduced neuronal models.	Supports the use of a single-compartment MSN framework and baseline electrophysiological parameter ranges.	Contextual modeling support	Supports model structure and plausibility, rather than direct validation of the A2A–cAMP–K^+ pathway.

Reference	Key finding from cited study	What it supports in the present model	Type of support	Scope of inference
(Moyer et al., 2007)[9], (Nair and Chakravarthy, 2024)[18]	Computational and systems-level studies support the use of simplified neuronal models for studying PD-related dynamics.	Supports the value of the present reduced model as a mechanism-isolation framework that may inform broader future modeling efforts.	Contextual modeling support	Supports the computational framing of the study, but not the specific biochemical-to-conductance coupling itself.

model approximates the passive electrophysiological regime of medium spiny neurons sufficiently to support comparative analysis across conditions, with the elevated R_in reflecting the simplified single-compartment geometry. Importantly, VmAvg values reported below represent mean membrane potentials during current injection (100– 250 ms) and are not resting potentials.

The results of the simulations conducted under Parkinson's disease (PD) and control conditions, including both the baseline and A2A receptor activation scenarios, are summarized in Table 3.

Membrane Potential and Excitability

The run-level data in Table 3 revealed clear between-condition differences in VmAvg, defined here as the mean membrane potential over the 100–250 ms during-stimulus window. Parkinson's untreated condition displays a pronounced hyperpolarization of the average membrane potential (mean = -15.3 mV), suggesting a reduction in neuronal excitability. Hyperpolarization was observed exclusively in the dopamine-depleted condition with active A2A signaling. Conversely, Control Baseline (mean ≈ -6.95 mV) and PD + Istradefylline (mean = -6.9 mV) conditions maintained a more depolarized mean membrane potential during stimulation, consistent with higher excitability under the injection protocol. While dopamine depletion in the Parkinson's Untreated state leads to hyperpolarized and less excitable neuron, the simulations of an A2A receptor antagonism (Istradefylline) restores membrane potential closer to the control state. These values represent VmAvg, the mean membrane potential during the 100–250 ms stimulus window, and not the resting membrane potential.

Modulated Potassium Conductance and Current

Changes in membrane potential were directly correlated with adjustments in the average steady-state modulated potassium conductance (gmodavg) and the resulting average potassium current (iKavg). In Parkinson's Untreated condition,

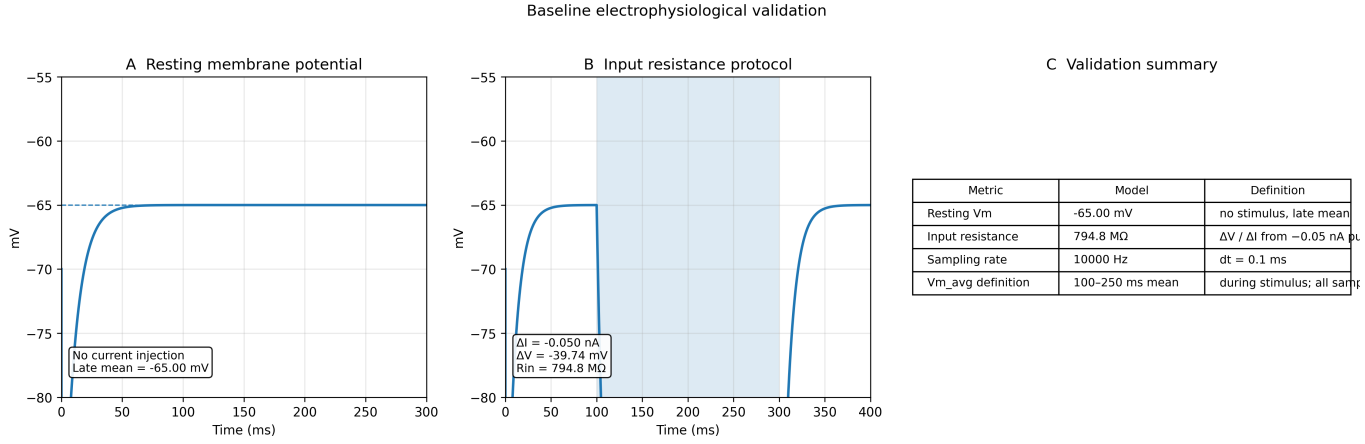

Figure. 2 Baseline electrophysiological validation of the model. (A) Resting membrane potential trace in the absence of current injection, demonstrating stable convergence to approximately 65 mV, consistent with the passive leak reversal potential and within experimentally reported ranges for medium spiny neurons. (B) Input resistance measurement using a hyperpolarizing current step (0.05 nA). The resulting steady-state voltage deflection (ΔV) relative to baseline was used to compute input resistance (Rin = $\Delta V / \Delta I$), yielding an approximate value of $795 M\Omega$. (C) Summary of baseline validation metrics, including resting membrane potential, input resistance, simulation sampling rate (dt = 0.1 ms; 10 kHz), and definition of Vmavg (mean membrane potential over 100–250 ms during stimulus, including all recorded samples).

Table 2 Model Parameters and Justifications.

Parameter Name	Description	Value	Units	Source / Justification
Passive Properties				
C_m	Specific membrane capacitance	1	μF/cm^2	Set in script; standard neuronal value
R_a	Axial resistance	100	Ω·cm	Set in script; typical for neuronal processes
g_{pas}	Passive (leak) conductance	1×10^{-4}	S/cm^2	Set in script; tuned to achieve resting membrane potential
E_{pas}	Passive (leak) reversal potential	-65	mV	Set in script; tuned to achieve resting membrane potential
R_{in}	Input resistance (whole-cell)	795	MΩ	Derived from soma geometry (20 μm $\times$ 20 μm cylinder) and passive conductance
E_{rest}	Resting membrane potential	-65	mV	Corresponds to passive leak reversal potential (E_{pas}) in absence of active currents
Active Ion Channels				
$g_{k,\text{bar}}$	Baseline maximum potassium conductance	0.05	S/cm^2	From NMODL script
e_K	Potassium reversal potential	-90	mV	Standard physiological value
n_q	Gating exponent for potassium current	4	–	From NMODL script
cAMP Signaling Pathway				
basal_cAMP_prod	Basal cAMP production rate	0.1	/ms	From NMODL script (ensures stable baseline)
deg_rate	cAMP degradation rate	0.1	/ms	From NMODL script; consistent with cAMP turnover rates
prod_rate	A2A-driven cAMP production rate (DA loss)	1.0	/ms	From NMODL script; represents upregulated signaling
base_cAMP	Baseline cAMP concentration for modulation	1	dimensionless (normalized)	From NMODL script; literature estimates of basal striatal cAMP
pd_cAMP_gain	Sensitivity of conductance to cAMP	5.0	unitless scaling factor	From NMODL script; represents facilitation strength

gmodavg was markedly elevated (mean = 0.55 S/cm²), and was associated with a shift in potassium current consistent with increased conductance during stimulation (mean = 0.011 mA/cm²). This increased potassium conductance acts to drive the membrane potential towards more negative values, explaining the observed hyperpolarization. Elevated potassium conductance was observed exclusively in the PD + A2A ON condition (mean g_mod $\approx 0.55 S/cm^2$), while all other conditions remained near baseline ($\approx 0.05 S/cm^2$). Conversely, in both the Control Baseline (mean gmodavg = $0.051 S/cm^2$, mean iKavg = $0.010 mA/cm^2$) and PD + Istradefylline (mean gmodavg = $0.051 S/cm^2$, mean iKavg = $0.010 mA/cm^2$) conditions, gmodavg and iKavg were substantially lower, contributing to their more depolarized membrane potentials.

cAMP Dynamics

Steady-state intracellular cAMP levels were condition-dependent and tightly constrained by dopamine status. In Parkinson's untreated condition with active A2A signaling, cAMP increased markedly to a steady-state mean of approximately 3.0 (normalized units) across trials. In contrast, Control Baseline, Control + A2A ON, and PD + Istradefylline conditions all maintained stable baseline cAMP levels near 1.0 (normalized units), consistent with the model formulation in which A2A-driven cAMP production is gated by dopamine

Table 3 Run-level simulation outputs for potassium-current modulation in Parkinson's disease and control conditions. VmAvg, IKAvg, GmodAvg, and cAMPAvg are during-stimulus averages computed over 100–250 ms during the current-injection protocol. VmAvg values represent mean membrane potential during the stimulus window and should not be interpreted as resting membrane potentials. Stimulus amplitude values reflect the per-run realized current injection amplitude after Gaussian jitter (mean 0.2 nA, σ = 0.005 nA) and should not be interpreted as the nominal protocol current

Scenario	Run	V_m Avg (mV; 100–250 ms)	I_K Avg (mA/cm^2; 100–250 ms)	G_{mod} Avg (S/cm^2; 100–250 ms)	cAMP Avg (normalized units; 100–250 ms)	Stimulus amplitude (nA)
PD + A2A ON	1	-15.373	0.011	0.55	3.00	0.1967
PD + A2A ON	2	-15.362	0.011	0.55	3.00	0.1971
PD + A2A ON	3	-15.239	0.011	0.55	3.00	0.2021
PD + A2A ON	4	-15.483	0.01	0.55	3.00	0.1923
PD + A2A ON	5	-15.585	0.01	0.55	3.00	0.1884
PD + A2A ON	6	-15.285	0.011	0.55	3.00	0.2002
PD + A2A ON	7	-15.199	0.011	0.55	3.00	0.2038
PD + A2A ON	8	-15.171	0.011	0.55	3.00	0.205
PD + A2A ON	9	-15.394	0.011	0.55	3.00	0.1958
PD + A2A ON	10	-15.38	0.011	0.55	3.00	0.1964
PD + A2A ON	11	-15.196	0.011	0.55	3.00	0.2039
PD + A2A ON	12	-15.227	0.011	0.55	3.00	0.2026
PD + A2A ON	13	-15.366	0.011	0.55	3.00	0.1969
PD + A2A ON	14	-15.16	0.011	0.55	3.00	0.2054
PD + A2A ON	15	-15.248	0.011	0.55	3.00	0.2017
PD + A2A ON	16	-15.286	0.011	0.55	3.00	0.2002
PD + A2A ON	17	-15.37	0.011	0.55	3.00	0.1968
PD + A2A ON	18	-15.189	0.011	0.55	3.00	0.2042
PD + A2A ON	19	-15.163	0.011	0.55	3.00	0.2053
PD + A2A ON	20	-15.278	0.011	0.55	3.00	0.2005
PD + Istradefylline	1	-6.559	0.011	0.05	1	0.2103
PD + Istradefylline	2	-6.777	0.01	0.05	1	0.2032
PD + Istradefylline	3	-6.762	0.01	0.05	1	0.2036
PD + Istradefylline	4	-6.831	0.01	0.05	1	0.2014
PD + Istradefylline	5	-6.776	0.01	0.05	1	0.2032
PD + Istradefylline	6	-6.875	0.01	0.05	1	0.2
PD + Istradefylline	7	-6.99	0.01	0.05	1	0.1964
PD + Istradefylline	8	-7.201	0.009	0.05	1	0.1901
PD + Istradefylline	9	-6.836	0.01	0.05	1	0.2013
PD + Istradefylline	10	-6.949	0.01	0.05	1	0.1977

PD + Istradefylline	11	-6.715	0.01	0.05	1	0.2052
PD + Istradefylline	12	-6.873	0.01	0.05	1	0.2001
PD + Istradefylline	13	-6.936	0.01	0.05	1	0.1981
PD + Istradefylline	14	-6.537	0.011	0.05	1	0.2111
PD + Istradefylline	15	-6.893	0.01	0.05	1	0.1995
PD + Istradefylline	16	-6.786	0.01	0.05	1	0.2029
PD + Istradefylline	17	-6.764	0.01	0.05	1	0.2036
PD + Istradefylline	18	-6.682	0.01	0.05	1	0.2062
PD + Istradefylline	19	-6.703	0.01	0.05	1	0.2056
PD + Istradefylline	20	-6.893	0.01	0.05	1	0.1995
Control + A2A ON	1	-6.824	0.01	0.05	1	0.2017
Control + A2A ON	2	-6.71	0.01	0.05	1	0.2053
Control + A2A ON	3	-6.974	0.01	0.05	1	0.1969
Control + A2A ON	4	-6.997	0.01	0.05	1	0.1962
Control + A2A ON	5	-6.91	0.01	0.05	1	0.1989
Control + A2A ON	6	-6.748	0.01	0.05	1	0.2041
Control + A2A ON	7	-6.938	0.01	0.05	1	0.198
Control + A2A ON	8	-6.839	0.01	0.05	1	0.2012
Control + A2A ON	9	-6.986	0.01	0.05	1	0.1966
Control + A2A ON	10	-6.998	0.01	0.05	1	0.1962
Control + A2A ON	11	-6.992	0.01	0.05	1	0.1964
Control + A2A ON	12	-7.056	0.01	0.05	1	0.1944
Control + A2A ON	13	-6.621	0.011	0.05	1	0.2083
Control + A2A ON	14	-6.829	0.01	0.05	1	0.2015
Control + A2A ON	15	-7.112	0.009	0.05	1	0.1927
Control + A2A ON	16	-6.677	0.01	0.05	1	0.2064
Control + A2A ON	17	-6.833	0.01	0.05	1	0.2014
Control + A2A ON	18	-6.96	0.01	0.05	1	0.1974
Control + A2A ON	19	-6.774	0.01	0.05	1	0.2033
Control + A2A ON	20	-6.921	0.01	0.05	1	0.1986
Control Baseline	1	-6.999	0.01	0.05	1	0.1962
Control Baseline	2	-6.871	0.01	0.05	1	0.2002
Control Baseline	3	-6.851	0.01	0.05	1	0.2008
Control Baseline	4	-6.955	0.01	0.05	1	0.1975
Control Baseline	5	-7.113	0.009	0.05	1	0.1927
Control Baseline	6	-6.85	0.01	0.05	1	0.2008
Control Baseline	7	-7.07	0.01	0.05	1	0.194
Control Baseline	8	-6.866	0.01	0.05	1	0.2003
Control Baseline	9	-7.184	0.009	0.05	1	0.1906
Control Baseline	10	-6.8	0.01	0.05	1	0.2024
Control Baseline	11	-7.02	0.01	0.05	1	0.1955
Control Baseline	12	-7.107	0.009	0.05	1	0.1929
Control Baseline	13	-6.91	0.01	0.05	1	0.1989
Control Baseline	14	-6.902	0.01	0.05	1	0.1992
Control Baseline	15	-6.648	0.011	0.05	1	0.2074
Control Baseline	16	-6.902	0.01	0.05	1	0.1992
Control Baseline	17	-6.828	0.01	0.05	1	0.2015

Control Baseline	18	-6.74	0.01	0.05	1	0.2044
Control Baseline	19	-7.313	0.009	0.05	1	0.1868
Control Baseline	20	-7.047	0.01	0.05	1	0.1947

depletion.

Descriptive Comparison Across Simulation Runs

Across the 20 simulation runs per condition, the ordering of outputs was stable under the imposed current jitter. The PD + A2A ON condition showed a more negative mean membrane potential during the stimulus window than the control and PD + Istradefylline conditions, together with higher mean g_mod, i_K, and cAMP. Effect-size analysis showed that the omnibus condition effect was extremely large for membrane potential (η^2=0.9986), modulated potassium conductance (η^2=1.0000), and cAMP (η^2=1.0000), and large for potassium current (η^2=0.5444). For the biologically central pairwise contrasts, PD + A2A ON showed extremely large separation from Control Baseline for Vm (Cohen's d=−60.23) and a large separation for IK (Cohen's d=2.57). Similarly, PD + A2A ON showed extremely large separation from PD + Istradefylline for Vm (Cohen's d=−63.70) and a large separation for IK (Cohen's d=2.40). For gmod and cAMP, within-condition variance was effectively zero in the run-level outputs, so Cohen's d was not informative; these effects are therefore better represented by η^2 together with the observed raw mean differences. In contrast, Control Baseline, Control + A2A ON, and PD + Istradefylline remained closely clustered for these metrics. We therefore interpret the between-condition separation descriptively, using mean values, run-to-run variability, and pairwise mean differences, rather than as population-level statistical significance. Trial-to-trial variability across the 20 runs per condition was low. For VmAvg, the coefficient of variation ranged from 0.75% in PD + A2A ON to 2.29% in Control Baseline. For IKAvg, CV ranged from 2.82% to 4.97% across conditions. In contrast, GmodAvg and cAMPAvg showed effectively zero within-condition CV in the present model output, reflecting that these variables converged to fixed condition0.010mA/cm^2) conditions, GmodAvg and IKAvg were substantially lower, contributing to by dopamine status. In PD + A2A ON condition with active A2A signaling, cAMP Conversely, in both the Control Baseline (mean GmodAvg =0.05S/cm^2, mean IKAvg = 0.010mA/cm^2) and PD + Istradefylline (mean GmodAvg = 0.05S/cm^2, mean IKAvg = specific steady-state values under the deterministic implementation. These findings indicate that the qualitative ordering of conditions was stable under the imposed small current jitter and that 20 trials per condition were sufficient to characterize withinprotocol variability for the reported metrics. Group-level distributions and post-hoc comparisons for V_m, I_K, g_mod, and cAMP are summarized in Figure 3. Representative time-course traces of membrane potential and potassium current for the same stimulation protocol are shown in Figure 4.

Sensitivity Analysis of pd_cAMP_gain

A local sensitivity analysis was performed by varying pd_cAMP_gain from 0 to 10 while holding all other parameters fixed. As expected from the model formulation, increasing pd_cAMP_gain selectively increased GmodAvg and shifted VmAvg toward more negative values in the PD + A2A ON condition, while the control-like conditions remained largely unchanged. For pd_cAMP_gain > 0, the qualitative ordering of conditions was preserved, with PD + A2A ON showing the most negative mean membrane response. At pd_cAMP_gain = 0, this separation disappeared, consistent with removal of the cAMP-dependent conductance coupling.

Model Validation

Simulation results are supported by a tiered validation framework in which some cited studies provide direct support for the modeled A2A–cAMP–excitability relationships, whereas others provide indirect translational or contextual support for the broader disease and modeling framework. The model's mechanistic behavior, particularly the modulation of cAMP dynamics and potassium current, supports insights from in vitro electrophysiological and biochemical studies[3,5,15]. The observed restoration of membrane potential and neuronal excitability by A2A antagonism in the model reflects the beneficial effects observed in clinical trials with istradefylline[21] and is consistent with altered neuronal activity reported in in vivo human electrophysiological studies (e.g., PNAS human striatal recordings[17]). These findings collectively provide contextual validation for the model's innovation in simulating intricate receptor-mediated signaling within computational neuroscience frameworks[4,18], providing an example for its ability to combine molecular mechanisms with system-level physiological changes.

Discussion

This computational study investigated how adenosine A2A receptor activity, represented within a reduced single-compartment medium spiny neuron model, influences somatic

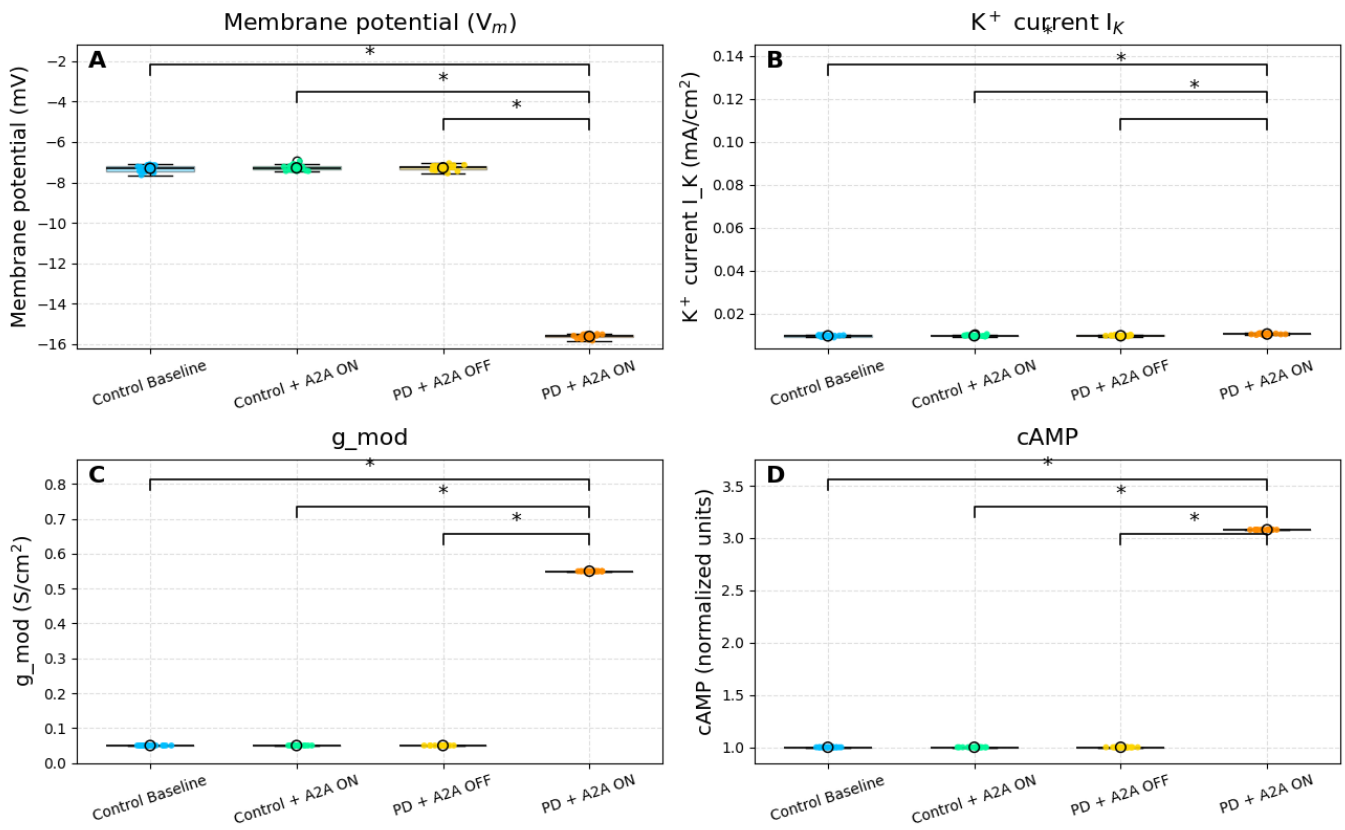

Figure. 3 Run-level summary of model outputs across conditions. Per-run values are shown for (A) membrane potential (V_m), (B) K^+ current (I_K), (C) modulated K^+ conductance (g_mod), and (D) intracellular cAMP. Points represent individual simulation runs under small injected-current jitter; horizontal bars indicate condition means.

membrane responses under Parkinsonian conditions. Under the specific assumptions and stimulation protocol used here, the simulations showed a clear mechanistic cascade: A2A activation in the dopamine-depleted condition increased cAMPAvg to approximately 3.0 normalized units, which increased the modeled potassium conductance (GmodAvg = $0.55 S/cm^2$). In this model, that conductance increase was associated with a more negative mean membrane potential during the stimulus window (VmAvg = 15.3 mV), consistent with reduced intrinsic excitability under the applied current injection. Within the model, simulated A2A antagonism (PD + Istradefylline) shifted these outputs toward control-like values. These findings therefore support a mechanism-level interpretation within the reduced model framework, rather than a complete account of MSN physiology in vivo.

It is important to contextualize the direction of the modeled excitability change within the known cell-type specificity of striatal circuitry. The hyperpolarization observed in the PD + A2A ON condition — a more negative mean membrane potential during current injection, associated with elevated K^+ conductance — reflects reduced intrinsic excitability at the single-cell somatic level under the applied depolarizing drive. This is consistent with the established indirect-pathway physiology: A2A receptors are preferentially expressed on indirect-pathway medium spiny neurons (iMSNs)[4,6,14], and increased A2A/cAMP signaling under dopamine depletion is understood to suppress iMSN excitability relative to baseline, which in turn disinhibits downstream targets and ultimately increases thalamo-cortical drive — contributing to the bradykinesia and motor suppression characteristic of Parkinson's disease. The systems-level consequence of this cellular suppression is therefore network-level hyperactivity in outputs such as GPi/SNr, consistent with the abnormal discharge patterns reported in human striatal recordings. The present model cap-

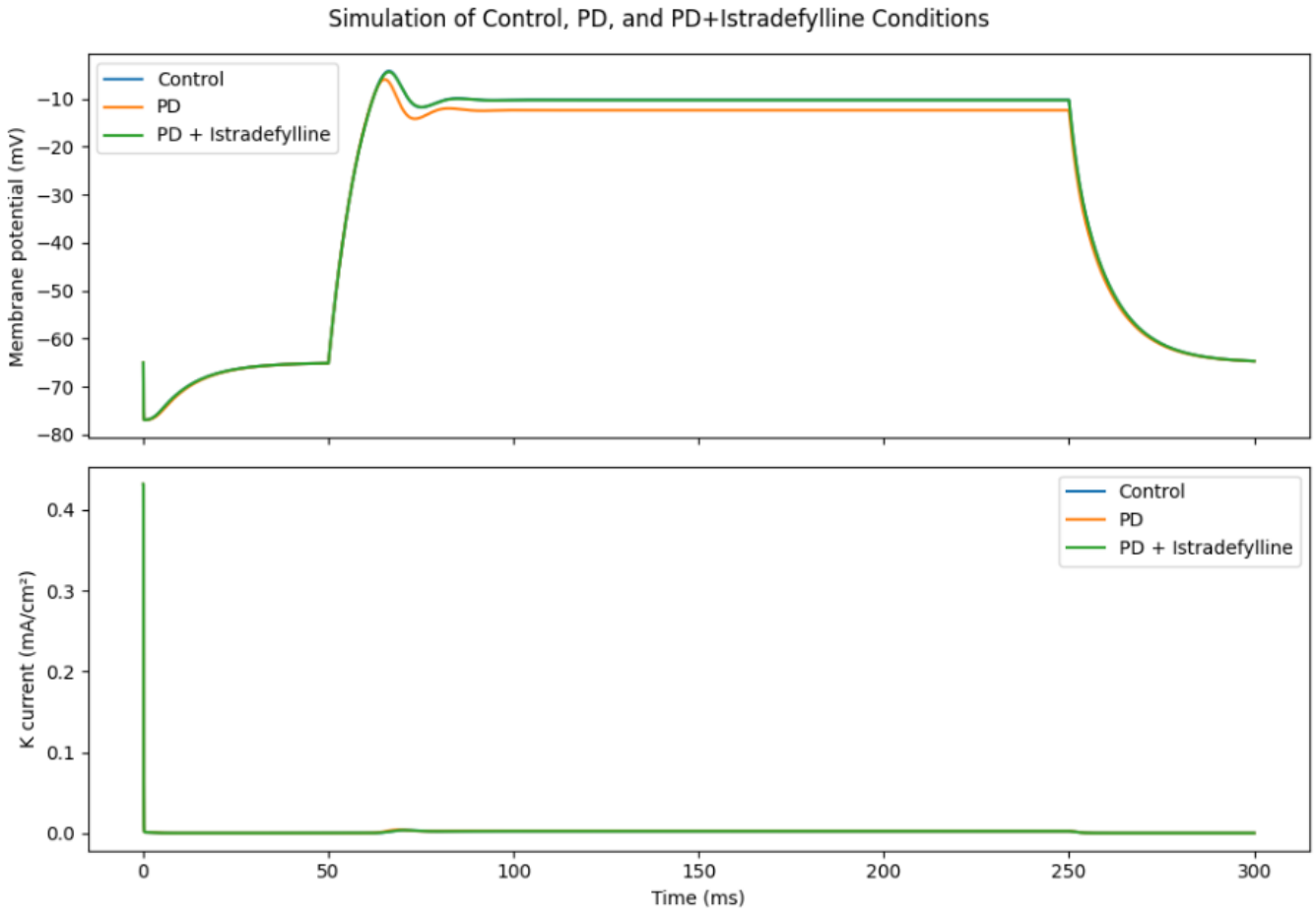

Figure. 4 Representative membrane potential and potassium current responses under Control Baseline, PD + A2A ON, and PD + Istradefylline conditions. Top: membrane potential (mV) over time (ms) during the stimulation protocol. Bottom: corresponding potassium current density (mA/cm^2). Traces illustrate the time course of the response and the relative separation among conditions during the depolarized plateau, with PD showing a slightly more negative plateau and PD + istradefylline shifting toward the control response.

tures the cellular upstream step — reduced iMSN intrinsic excitability — and does not model the network-level consequence. Claims about the model's consistency with human electrophysiological recordings therefore refer to the directional plausibility of the pathway rather than to a direct comparison of single-unit firing rates. This distinction is important: the model supports the mechanistic interpretation that A2A–cAMP-dependent K^+ conductance elevation suppresses iMSN responsiveness, but it does not itself demonstrate the downstream hyperactivity that is the proximal cause of PD motor symptoms.

Compared to existing models of the striatum and Parkinson's disease, this model introduces several innovations. It explicitly incorporates adenosine A2A receptor signaling and its downstream effects on intracellular cAMP dynamics, which have been absent from prior frameworks focusing on dopaminergic modulation. It mechanistically links receptor activation to potassium channel conductance via a dynamic cAMP-dependent modulation, providing a biochemical-to-electrophysiological bridge that most models treat phenomenologically. Parkinsonian conditions are represented through a dopamine-depletion toggle that dynamically disinhibits A2A-mediated signaling, enabling direct simulation of disease-state physiology. Finally, the model includes pharmacological modulation (A2A antagonism) and is validated against multiple experimental scales, from molecular data to clinical effects of istradefylline. These features collectively establish this model as a novel mechanistic framework that integrates receptor-level signaling with electrophysiological outcomes relevant to Parkinson's disease.

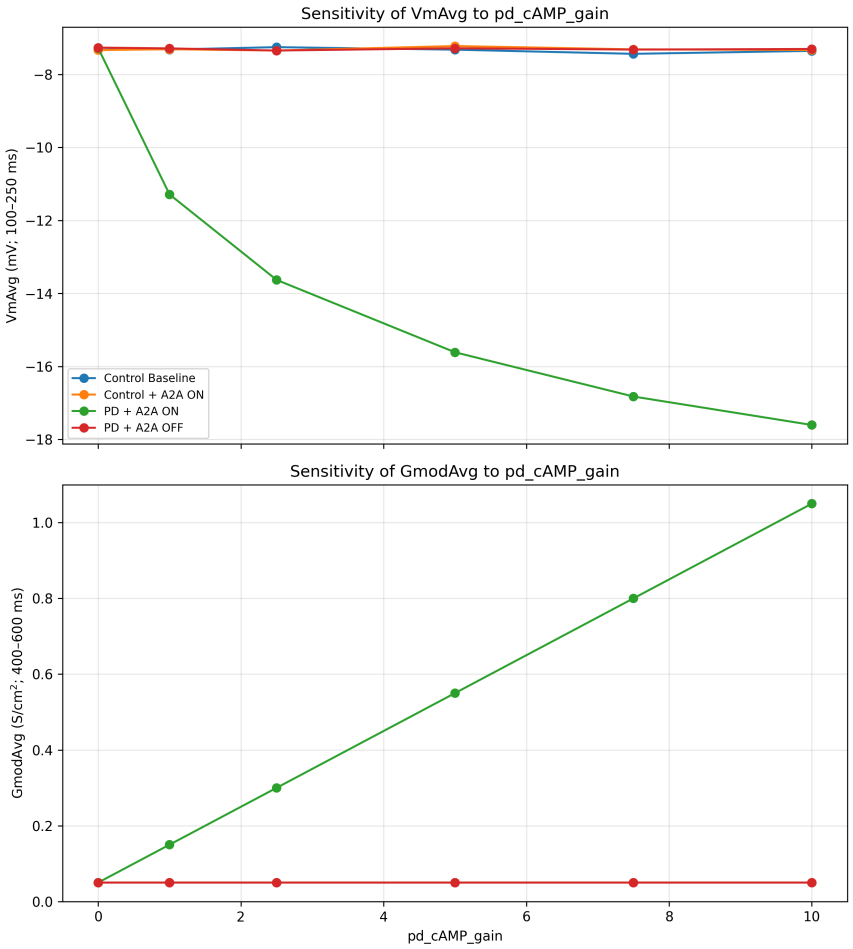

Figure. 5 Sensitivity of model outputs to pd_cAMP_gain. Varying pd_cAMP_gain selectively altered GmodAvg and VmAvg in the PD + A2A ON condition, while control-like conditions remained largely unchanged. For pd_cAMP_gain > 0, the qualitative ordering of conditions was preserved.

Mechanistic Interpretation and In Vitro Validation

The model's core validity rests on the convergence of its simulated molecular and biophysical changes established in vitro findings. The notable elevation in cAMPavg in the Parkinson's Untreated state confirms the model's structure, which posits that the loss of inhibitory D2 receptor tone in the dopamine-depleted environment disinhibits the A2A-mediated cAMP production pathway. This aligns directly with experimental evidence from human post-mortem studies showing increased A2A receptor levels in the striatum of PD patients[3], providing the molecular basis for increased signaling. Furthermore, the underlying mechanism is supported by the existence of A2A-D2 receptor heterotetramers and their physical coupling to adenylyl cyclase[22], as exhibited by Ferré and colleagues[4,8] which explains why A2A signaling effectively dominates when dopamine levels drop[4,23].

The resulting increase in cAMP was associated with a significant increase in K^+ conductance (gmodavg), consistent with the model's hypothesis that A2A signaling facilitates potassium channel opening; however, this coupling is represented phenomenologically rather than through an explicit intermediate kinase cascade. This finding is consistent with reports that postsynaptic A2A receptor activity can regulate intrinsic excitability via ion-channel conductance changes[15]. This conductance increase links the A2A pathway to other key striatal signaling molecules, such as DARPP-32, which is influenced by A2A activity and is known to modulate K^+ channels[4]. Therefore, the model successfully links molecular receptor activation to a specific biophysical consequence: heightened potassium efflux.

Translational Relevance and In Vivo/Clinical Validation

The most physiologically relevant result is the hyperpolarization of the membrane potential (Vmavg = −15.3 mV) observed in Parkinson's Untreated condition. Because all conditions were evaluated under the same current-step protocol, these results support a comparative claim about relative intrinsic excitability under matched depolarizing drive rather than a full characterization of the neuron's frequency–current input–output relationship. These are average membrane potentials during sustained current injection, not resting potentials. This is consistent with electrophysiological observations from the field, which report altered firing patterns and pathological discharge in striatal projection neurons recorded in vivo in human PD patients [17]. Within the model, the more negative membrane response under the PD + A2A ON condition is quantitatively linked to the imposed increase in A2A-mediated potassium conductance. This should be interpreted as a mechanism-level result under the assumptions of the reduced model, not as direct proof that the same causal weighting applies in biological neurons or patients. The A2A–cAMP pathway was simplified into a first-order differential equation for cAMPAvg, and the link between cAMP and K^+ conductance was modeled phenomenologically, omitting the explicit representation of intermediate signaling molecules such as PKA and DARPP-32.

Within the model, the shift of these simulated physiological parameters toward control-like values in the PD + Istradefylline condition provides support for the internal consistency of the modeled mechanism and is qualitatively consistent with the therapeutic rationale for A2A antagonism; however, it does not constitute direct evidence of treatment efficacy or mechanism in biological neurons or patients. This result is consistent with the established clinical efficacy of istradefylline [2,24] and suggests one possible cellular mechanism by which A2A antagonism could shift modeled membrane behavior toward control-like values.

More cautiously, the model supports the inference that reducing A2A-driven signaling could shift modeled membrane behavior toward a more control-like state [25] under dopamine-depleted conditions. Any implication for clinical improvement remains indirect and depends on external experimental and clinical evidence rather than on the simulations alone.

Context within Computational Modeling

This study contributes a detailed, multi-validated cellular mechanism to the computational neuroscience community. While built upon established parameters for the PD state [12], the present work innovates by integrating dynamic, receptor-mediated second messenger kinetics (cAMPavg) to modulate ion channel conductance (GmodAvg). This level of molecular detail may be useful for improving the biological specificity of future larger-scale network models, although the present study itself does not test network behavior. For instance, the resulting hyperpolarization predicted here can be integrated into broader basal ganglia models [18] to accurately simulate the consequences of dopamine depletion on system output and motor symptoms. Furthermore, this refined single-cell model serves as a necessary component for future work aimed at reproducing in vivo phenomena, such as pathological LFP oscillations observed in human DBS patients [19,26].

Study Limitations and Future Directions

The primary limitation of this study is the use of a single-compartment model, which necessarily simplifies the complex electrophysiology of the striatal medium spiny neuron. In addition, excitability was assessed primarily using a single matched current-step protocol rather than a full current-amplitude sweep, so the model is best interpreted as demonstrating condition-dependent differences in relative excitability under standardized stimulation. A single-compartment framework cannot account for heterogeneous channel distribution, compartmentalized signaling cascades, or the integration of synaptic inputs necessary for realistic spiking behavior. Additionally, the A2A–cAMP pathway was simplified into a first-order differential equation for cAMPavg, and the link between cAMP and K^+ conductance was modeled phenomenologically, omitting the explicit representation of intermediate signaling molecules such as PKA and DARPP-32.

An additional limitation is that the present model represents MSN intrinsic excitability with one simplified cAMP-sensitive potassium mechanism rather than the full complement of potassium currents expressed by medium spiny neurons. Accordingly, the modeled current should be interpreted as a reduced delayed-rectifier-like surrogate for potassium-mediated intrinsic-excitability changes in MSNs, not as a definitive simulation of any single native K^+ channel subtype. In biological MSNs, multiple K^+ conductances contribute to resting membrane potential, repolarization, subthreshold integration, and responsiveness to injected current. Of those, inwardly rectifying K^+ currents (Kir2 family) tend to stabilize the membrane at hyperpolarized potentials and would likely amplify the direction of the modeled effect, while A-type K^+ currents (Kv4 family) activate transiently during early depolarization and could partially offset the delayed-rectifier-mediated hyperpolarization, thereby reducing its magnitude. Because those parallel currents were not explicitly represented here, the magnitude of the simulated hyperpolarization should be interpreted as mechanism-specific rather than as a complete quantitative prediction of total MSN behavior; however, the sustained outward direction of the modeled K^+ effect is robust to this uncertainty. Recent work further indicates that A2A signaling operates within a broader striatal signaling [27] land-

scape that includes receptor heteromers, astrocytic A2A–D2 interactions, and celltype-specific signaling adaptations[28,29]; these developments support the relevance of the modeled pathway while also underscoring that the present neuron-centered, phenomenological framework captures only one tractable subset of that biology. Accordingly, this model is best understood as isolating one plausible contributor to reduced excitability under dopamine depletion, not as claiming that this single current alone fully determines the electrophysiological phenotype of Parkinsonian MSNs.

Future work should focus on expanding this mechanism into a multi-compartment MSN model to investigate how A2A-mediated modulation of K^+ conductance affects dendritic integration and spiking patterns. Moreover, incorporating other key ion channels and receptor systems into the gmod framework will allow for more nuanced simulations of pharmaceutical interventions and the pathological emergence of network-level phenomena, such as the pathological rhythmicity observed in PD.

Conclusion

Under the assumptions of this single-compartment model, A2A receptor upregulation during dopamine depletion increased a modeled cAMP-sensitive potassium conductance and shifted the somatic membrane response toward more negative values during current injection. The reversal of that shift by simulated A2A antagonism supports the interpretation that A2A–cAMP-dependent potassium modulation may contribute to reduced excitability in Parkinsonian conditions, but the model does not by itself establish the full electrophysiological phenotype of medium spiny neurons in vivo. Beyond reproducing condition-dependent trends within this reduced framework, the model integrates A2A receptor signaling, cAMP dynamics, and potassium channel modulation in a way that may be useful for future multi-compartment and network-level studies of Parkinson's disease.

Acknowledgments

The author would like to thank her peers for their guidance and support.

References

1 D. Karati, S. Mukherjee, S. Roy. Molecular and structural insight into adenosine a2a receptor in neurodegenerative disorders: a significant target for efficient treatment approach. Molecular Neurobiology. Vol. 60, pg. 5987–6000, 2023, https://doi.org/10.1007/s12035-023-03441-5.

2 P. A. LeWitt, M. Guttman, J. W. Tetrud, P. J. Tuite, A. Mori, P. Chaikin, N. M. Sussman, 6002-US-005 Study Group. Adenosine a2a receptor antagonist istradefylline (kw-6002) reduces "off" time in parkinson's disease: a double-blind, randomized, multicenter clinical trial (6002-us-005). Annals of Neurology. Vol. 63, pg. 295–302, 2008, https://doi.org/10.1002/ana.21315.

3 F. Calon, M. Dridi, O. Hornykiewicz, P. J. Bédard, A. H. Rajput, T. Di Paolo. Increased adenosine a2a receptors in the brain of parkinson's disease patients with dyskinesias. Brain. Vol. 127, pg. 1075–1084, 2004, https://doi.org/10.1093/brain/awh128.

4 S. Ferré, J. Bonaventura, W. Zhu, C. Hatcher-Solis, J. Taura, C. Quiroz, N.-S. Cai, E. Moreno, V. Casadó-Anguera, A. V. Kravitz, K. R. Thompson, D. G. Tomasi, G. Navarro, A. Cordomí, L. Pardo, C. Lluís, C. W. Dessauer, N. D. Volkow, V. Casadó, F. Ciruela, D. E. Logothetis, D. Zwilling. Essential control of the function of the striatopallidal neuron by pre-coupled complexes of adenosine a2a-dopamine d2 receptor heterotetramers and adenylyl cyclase. Frontiers in Pharmacology. Vol. 9, 2018, https://doi.org/10.3389/fphar.2018.00243.

5 H.-Y. Shen, P. M. Canas, P. Garcia-Sanz, J.-Q. Lan, D. Boison, R. Moratalla, R. A. Cunha, J.-F. Chen. Adenosine a2a receptors in striatal glutamatergic terminals and gabaergic neurons oppositely modulate psychostimulant action and darpp-32 phosphorylation. PLOS ONE. Vol. 8, pg. e80902, 2013, https://doi.org/10.1371/journal.pone.0080902.

6 S. Ferré, C. Quiroz, A. S. Woods, R. Cunha, P. Popoli, F. Ciruela, C. Lluis, R. Franco, K. Azdad, S. N. Schiffmann. An update on adenosine a2a-dopamine d2 receptor interactions: implications for the function of g protein-coupled receptors. Current Pharmaceutical Design. Vol. 14, pg. 1468–1474, 2008, https://doi.org/10.2174/138161208784480108.

7 P. Svenningsson, A. Nishi, G. Fisone, J.-A. Girault, A. C. Nairn, P. Greengard. DARPP-32: an integrator of neurotransmission. Annual Review of Pharmacology and Toxicology. Vol. 44, pg. 269–296, 2004, https://doi.org/10.1146/annurev.pharmtox.44.101802.121415.

8 S. Ferré, L. I. Sarasola, C. Quiroz, F. Ciruela. Presynaptic adenosine receptor heteromers as key modulators of glutamatergic and dopaminergic neurotransmission in the striatum. Neuropharmacology. Vol. 223, pg. 109329, 2023, https://doi.org/10.1016/j.neuropharm.2022.109329.

9 J. T. Moyer, J. A. Wolf, L. H. Finkel. Effects of dopaminergic modulation on the integrative properties of the ventral striatal medium spiny neuron. Journal of Neurophysiology. Vol. 98, pg. 3731–3748, 2007, https://doi.org/10.1152/jn.00335.2007.

10 M. L. Hines, N. T. Carnevale. The neuron simulation environment. Neural Computation. Vol. 9, pg. 1179–1209, 1997, https://doi.org/10.1162/neco.1997.9.6.1179.

11 T. S. Gertler, C. S. Chan, D. J. Surmeier. Dichotomous anatomical properties of adult striatal medium spiny neurons. The Journal of Neuroscience: The Official Journal of the Society for Neuroscience. Vol. 28, pg. 10814–10824, 2008, https://doi.org/10.1523/JNEUROSCI.2660-08.2008.

12 C. J. Wilson, Y. Kawaguchi. The origins of two-state spontaneous membrane potential fluctuations of neostriatal spiny neurons. The Journal of Neuroscience: The Official Journal of the Society for Neuroscience. Vol. 16, pg. 2397–2410, 1996, https://doi.org/10.1523/JNEUROSCI.16-07-02397.1996.

13 E. A. Rendón-Ochoa, M. Padilla-Orozco, V. M. Calderon, V. H. Avilés-Rosas, O. Hernández-González, T. Hernández-Flores, M. B. Perez-Ramirez, M. Palomero-Rivero, E. Galarraga, J. Bargas. Dopamine d2 and adenosine a2a receptors interaction on ca2+ current modulation in a rodent model of parkinsonism. ASN NEURO. Vol. 14, pg. 17590914221102075, 2022, https://doi.org/10.1177/17590914221102075.

14 R. Rivas-Santisteban, A. J. Rico, A. Muñoz, A. I. Rodríguez-Pérez, I. Reyes-Resina, G. Navarro, J. L. Labandeira-García, J. L. Lanciego, R. Franco. Boolean analysis shows a high proportion of dopamine d2 re-

ceptors interacting with adenosine a2a receptors in striatal medium spiny neurons of mouse and non-human primate models of parkinson's disease. Neurobiology of Disease. Vol. 188, pg. 106341, 2023, https://doi.org/10.1016/j.nbd.2023.106341.

15 A. R. Rau, O. J. Ariwodola, J. L. Weiner. Postsynaptic adenosine a2a receptors modulate intrinsic excitability of pyramidal cells in the rat basolateral amygdala. International Journal of Neuropsychopharmacology. Vol. 18, pg. pyv017, 2015, https://doi.org/10.1093/ijnp/pyv017.

16 F. S. Menniti, T. A. Chappie, C. J. Schmidt. PDE10A inhibitors-clinical failure or window into antipsychotic drug action? Frontiers in Neuroscience. Vol. 14, pg. 600178, 2020, https://doi.org/10.3389/fnins.2020.600178.

17 A. Singh, K. Mewes, R. E. Gross, M. R. DeLong, J. A. Obeso, S. M. Papa. Human striatal recordings reveal abnormal discharge of projection neurons in parkinson's disease. Proceedings of the National Academy of Sciences. Vol. 113, pg. 9629–9634, 2016, https://doi.org/10.1073/pnas.1606792113.

18 S. S. Nair, S. Chakravarthy. A computational model of deep brain stimulation for parkinson's disease tremor and bradykinesia. Brain Sciences. Vol. 14, pg. 620, 2024, https://doi.org/10.3390/brainsci14060620.

19 A. J. Baumgartner, C. A. Kushida, M. O. Summers, D. S. Kern, A. Abosch, J. A. Thompson. Basal ganglia local field potentials as a potential biomarker for sleep disturbance in parkinson's disease. Frontiers in Neurology. Vol. 12, pg. 765203, 2021, https://doi.org/10.3389/fneur.2021.765203.

20 A. L. Hodgkin, A. F. Huxley. A quantitative description of membrane current and its application to conduction and excitation in nerve. The Journal of Physiology. Vol. 117, pg. 500–544, 1952, https://doi.org/10.1113/jphysiol.1952.sp004764.

21 M.-C. Allichon, V. Ortiz, P. Pousinha, A. Andrianarivelo, A. Petitbon, N. Heck, P. Trifilieff, J. Barik, P. Vanhoutte. Cell-type-specific adaptions in striatal medium-sized spiny neurons and their roles in behavioral responses to drugs of abuse. Frontiers in Synaptic Neuroscience. Vol. 13, pg. 799274, 2021, https://doi.org/10.3389/fnsyn.2021.799274.

22 K. Prasad, E. F. J. de Vries, P. H. Elsinga, R. A. J. O. Dierckx, A. van Waarde. Allosteric interactions between adenosine a2a and dopamine d2 receptors in heteromeric complexes: biochemical and pharmacological characteristics, and opportunities for pet imaging. International Journal of Molecular Sciences. Vol. 22, pg. 1719, 2021, https://doi.org/10.3390/ijms22041719.

23 .-F. Chen, D.-S. Choi, R. A. Cunha. Striatopallidal adenosine a2a receptor modulation of goal-directed behavior: homeostatic control with cognitive flexibility. Neuropharmacology. Vol. 226, pg. 109421, 2023, https://doi.org/10.1016/j.neuropharm.2023.109421.

24 T. Müller. The role of istradefylline in the parkinson's disease armamentarium. Expert Opinion on Pharmacotherapy. Vol. 24, pg. 863–871, 2023, https://doi.org/10.1080/14656566.2023.2201374.

25 Y. Zhao, Y.-G. Zhou, J.-F. Chen. Targeting the adenosine a2a receptor for neuroprotection and cognitive improvement in traumatic brain injury and parkinson's disease. Chinese Journal of Traumatology = Zhonghua Chuang Shang Za Zhi. Vol. 27, pg. 125–133, 2024, https://doi.org/10.1016/j.cjtee.2023.08.003.

26 A. Cavallo, W.-J. Neumann. Dopaminergic reinforcement in the motor system: implications for parkinson's disease and deep brain stimulation. The European Journal of Neuroscience. Vol. 59, pg. 457–472, 2024, https://doi.org/10.1111/ejn.16222.

27 C. P. Garcia, A. Licht-Murava, A. G. Orr. Effects of adenosine a2a receptors on cognitive function in health and disease. International Review of Neurobiology. Vol. 170, pg. 121–154, 2023, https://doi.org/10.1016/bs.irn.2023.04.006.

28 C. Cervetto, G. Maura, D. Guidolin, S. Amato, C. Ceccoli, L. F. Agnati, M. Marcoli. Striatal astrocytic a2a-d2 receptor-receptor interactions and their role in neuropsychiatric disorders. Neuropharmacology. Vol. 237, pg. 109636, 2023, https://doi.org/10.1016/j.neuropharm.2023.109636.

29 J.-P. Roussarie, P. Rodriguez-Rodriguez. Deciphering cell-type specific signal transduction in the brain: challenges and promises. Advances in Pharmacology. Vol. 90, pg. 145–171, 2021, https://doi.org/10.1016/bs.apha.2020.09.009.